NF-Heart: A Near-field Non-contact Continuous User Authentication System via Ballistocardiogram

YANDAO HUANG, CSE, Hong Kong University of Science and Technology, China
MINGHUI QIU, DSA, Hong Kong University of Science and Technology (Guangzhou), China
LIN CHEN, DSA, Hong Kong University of Science and Technology (Guangzhou), China
ZHENCAN PENG, CSSE, Shenzhen University, China
QIAN ZHANG, CSE, Hong Kong University of Science and Technology, China
KAISHUN WU, DSA & IoT, Hong Kong University of Science and Technology (Guangzhou), China

The increasingly remote workforce resulting from the global coronavirus pandemic has caused unprecedented cybersecurity concerns to organizations. Considerable evidence has shown that one-pass authentication fails to meet security needs when the workforce work from home. The recent advent of continuous authentication (CA) has shown the potential to solve this predicament. In this paper, we propose NF-Heart, a physiological-based CA system utilizing a ballistocardiogram (BCG). The key insight is that the BCG measures the body's micro-movements produced by the recoil force of the body in reaction to the cardiac ejection of blood, and we can infer cardiac biometrics from BCG signals. To measure BCG, we deploy a lightweight accelerometer on an office chair, turning the common chair into a smart continuous identity "scanner". We design multiple stages of signal processing to decompose and transform the distorted BCG signals so that the effects of motion artifacts and dynamic variations are eliminated. User-specific fiducial features are then extracted from the processed BCG signals for authentication. We conduct comprehensive experiments on 105 subjects in terms of verification accuracy, security, robustness, and long-term availability. The results demonstrate that NF-Heart achieves a mean balanced accuracy of 96.45% and a median equal error rate of 3.83% for CA. The proposed signal processing pipeline is effective in addressing various practical disturbances.

CCS Concepts: • **Security and privacy** → **Biometrics**; • **Human-centered computing** → *Ubiquitous and mobile computing*.

Additional Key Words and Phrases: Continuous authentication; Ballistocardiogram (BCG); Biometrics; Non-contact sensing; Smart Chair;

ACM Reference Format:
Yandao Huang, Minghui Qiu, Lin Chen, Zhencan Peng, Qian Zhang, and Kaishun Wu. 2023. NF-Heart: A Near-field Non-contact Continuous User Authentication System via Ballistocardiogram. *Proc. ACM Interact. Mob. Wearable Ubiquitous Technol.* 7, 1, Article 16 (March 2023), 24 pages. https://doi.org/10.1145/3580851

Authors' addresses: Yandao Huang, yhuangfg@connect.ust.hk, CSE, Hong Kong University of Science and Technology, China; Minghui Qiu, mqiu585@connect.hkust-gz.edu.cn, DSA, Hong Kong University of Science and Technology (Guangzhou), China; Lin Chen, lchen297@connect.hkust-gz.edu.cn, DSA, Hong Kong University of Science and Technology (Guangzhou), China; Zhencan Peng, 2018152014@email.szu.edu.cn, CSSE, Shenzhen University, Shenzhen, China; Qian Zhang, qianzh@cse.ust.hk, CSE, Hong Kong University of Science and Technology, Hong Kong, China; Kaishun Wu, wuks@ust.hk, DSA & IoT, Hong Kong University of Science and Technology (Guangzhou), Hong Kong, China.

2474-9567/2023/3-ART16 $15.00
https://doi.org/10.1145/3580851

Fig. 1. Illustration of NF-Heart in a factory scenario. With BCG measurements from the chair, the workers can be secure remote workforce when sitting at home.

1 INTRODUCTION

The global coronavirus pandemic shifted tens of millions of workers from on site to remote work. [61] reported that 54% of organizations have adopted a work-from-home policy in response to COVID-19. With an increasingly remote workforce, the digital perimeter becomes proportionally porous and vulnerable. Enterprises and governments are facing unprecedented cybersecurity threats regarding equipment safety, data security, and privacy leakage. According to [12], the attacks on usernames and passwords have undergone staggering growth of 450% in 2020 from 2019, translating into more than one billion compromised records in the U.S.A. alone. This reveals that traditional authentication schemes like passwords or pattern locks are vulnerable and insecure. It is urgent to propose a reliable and trustworthy authentication scheme to verify the identity of the sit-at-home workforce.

Existing methods for CA can be categorized into two types. Behavioral biometrics-based CA systems leverage the gait [65], gaze [56, 70], touching [2, 13], and keystroke [47, 51] dynamics to characterize users, which relies on user involvement and limits to only a few application scenarios. Physiological biometrics-based CA systems build upon the recent advance in bio-signal detection of wearable devices (e.g., ECG [72] and PPG [8, 71]). However, these methods require direct skin contact for the measurement. Cardiac Scan [36] implements a novel non-contact CA system by capturing the cardiac deformation with a DC-couple continuous wave Doppler radar. RF-cardiography (RFG) detection needs expensive infrastructure and is error-prone in a dynamic environment. In addition, above mentioned physiological biometrics-based systems still maintain authorized access when the legal user presents nearby, providing a possible chance for the attacker to perform transient attacks.

In this paper, we propose NF-Heart, a secure and unobtrusive continuous authentication (CA) system based on near-field non-contact ballistocardiogram (BCG) measurements. Nowadays, the amount of time that a person is sitting has reached over 12 hours per day on average [26], accounting for around 75% of their awake time. In addition, literature has shown that that the workers spend around 80% of their working hours sitting [16, 45]. Therefore, we turn a common chair into an identity "scanner" by deploying a lightweight accelerometer on the chair. As shown in Figure 1, the system can continuously extract BCG biometrics for authentication when users are seated.

NF-Heart can provide greater security by monitoring user actions and verify the user's identity at every moment during a session. Even if an attacker has gained the legitimate user's credentials, NF-Heart can ensure the user is not impersonated at any time.

However, we need to tackle several challenges before transforming the above high-level ideas into practice: 1) The intrinsic heart rate variability and low power of BCG signals make segmentation and delineation rather challenging. 2) BCG is susceptible to motion artifacts (MAs) that will distort BCG morphology and lead to system failure. How can we eliminate the effects of arbitrary MAs and guarantee robust BCG measurement when deploying NF-Heart in the wild? 3) The unavoidable effects of respiration, sitting posture, user emotion, and sensor position on BCG signals are open issues that remain to be addressed [22]. The trained model may no longer be applicable for authentication when any of these factors changes. Is there a way to extract stable and invariant features from BCG?

To address these challenges, we first validate the uniqueness of BCG biometrics based on the BCG genesis model and explore the characteristics of BCG signals by analyzing the relationships between each fiducial point. Then, we propose to measure the instantaneous power of BCG signals for accurate heartbeat segmentation. We further develop a Hidden Signal Quality Index (H-SQI) for detecting arbitrary types of MAs. A two-stage MA-removal scheme is designed to recover the interfered BCG signals. The recovered signals are transformed into the angle domain with a dynamical BCG model to deal with multiple dynamic factors. After that, we propose a simplified U-net architecture to delineate 45 fiducial features and leverage a convolutional autoencoder (CAE) to verify users.

We evaluate NF-Heart on a BCG dataset collected from 105 subjects. Our evaluation shows that NF-Heart is a secure and trustworthy CA system that can verify users with a balanced accuracy (BAC) of 96.45% and an equal error rate (EER) of 3.83%. We also conduct extensive experiments to examine the robustness and availability of NF-Heart under various conditions. The results validate that NF-Heart can resist various practical disturbances and attacks.

The main contributions of NF-Heart are summarized as follows:

- We propose a near-field continuous user authentication system using unique BCG biometrics. Our system can guarantee the remote access security of organizations by continuously verifying the identity of work-at-home staff.
- We design multiple stages of signal processing to recover distorted BCG signals for practical authentication in actual situations. User-specific BCG features are successfully extracted using modified U-net architecture and CAE framework.
- We design a smart chair for non-contact BCG measurements. We conduct extensive experiments involving 105 subjects to validate the security, availability, and robustness of NF-Heart.

2 BACKGROUND

2.1 Background of BCG Signals

Ballistocardiogram (BCG) signals provide details of cardiac activity, and its measurement do not need to be obtained by attaching electrodes or sensors to the human body. There are considerable clinical research and applications regarding BCG, including heart/respiration-rate monitoring [3, 6], blood-pressure monitoring [27, 28], sleep-stage evaluation [20, 30], heart-rate variability (HRV) analyses [35, 53], infant monitoring in beds [32], and so on. The non-contact and convenience of BCG measurement make BCG a good choice as a substitute for electrocardiogram (ECG) in many scenarios.

Newton's third law of motion is the primary physical principle of a BCG. During a cardiac cycle, blood mass is ejected from the heart and passes through the vascular system. The blood flow is reflected by bodily motion in the opposite direction, which maintains balance in the system's overall gravity [49]. By recording the resultant micro-vibrations of the human body using specialized apparatus, we can obtain a BCG waveform, as shown in Figure 4. The BCG waves are named with capital letters G through N [57], with each letter representing a specific cardiac cycle event [46] as shown in Table 3 in the Appendix. The BCG morphology characterizes the entire

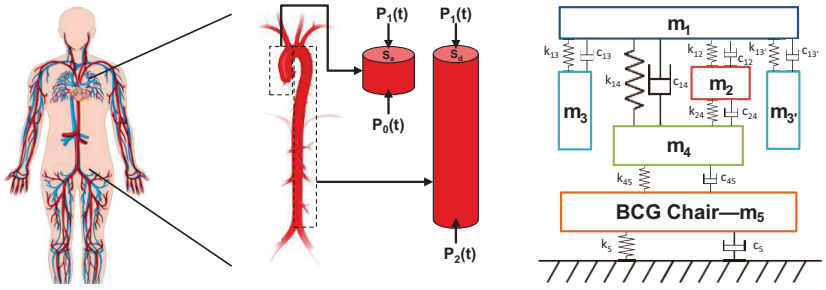

(a) Vascular tree of body (b) Aorta tubes for BCG genesis model (c) 6-DoF model

Fig. 2. Illustration of a vascular tree, BCG genesis model, and 6-DoF model for BCG.

Fig. 3. NF-Heart on a plastic chair.

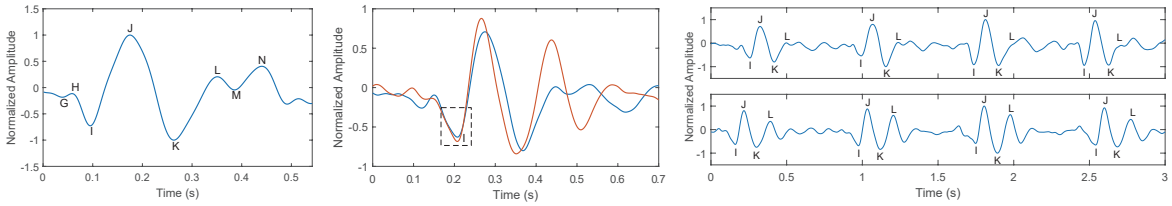

(a) A normal BCG waveform (b) Distinctness of BCG waveform (c) Consistency of BCG waveform

Fig. 4. (a) An example of a standard head-to-foot BCG waveform and the name of each component. A comparison of BCG waveforms from two subjects where (b) is one heartbeat cycle and (c) is four consecutive heartbeats.

process of cardiac deformation and can not be controlled by the subjective thought of individuals. The recoil force can be recorded as BCG signals whether the subject is standing, sitting, or lying flat [22].

2.2 BCG Genesis Model

As shown in Figure 2(a), the vascular tree of the human body is a very complicated system. Therefore, it is difficult for researchers to model the BCG waveforms and explain the underlying mechanisms mathematically. It was not until 2016 that the most well-acknowledged BCG genesis model was proposed by [29]. A BCG wave is estimated as an instantaneous force exerted on the blood in the main artery, as shown in Figure 2(b). In brief, the BCG force F_{BCG} can be mathematically expressed as:

$$F_{BCG}(t) = S_d[P_1(t) - P_2(t)] - S_a[P_0(t) - P_1(t)] \tag{1}$$

where S_d and S_a represent the average cross-sectional areas of the descending and ascending aorta, respectively, and $P_0(t)$, $P_1(t)$, and $P_2(t)$ are the blood pressure waves of the ascending aorta inlet, arch outlet/inlet, and descending aorta outlet, respectively. Based on this model, mechanistic insight for the genesis of BCG data is then interpreted as the blood-pressure gradients in the ascending and descending aorta.

We can further model head-to-foot BCG transmission in the body with a multiple degrees-of-freedom (DoF) spring–mass–damper model, as shown in Figure 2(c). The model consists of six mass elements indicating the upper torso (m_1), internal organs (m_2), upper limbs (m_3 and $m_{3'}$), lower limbs (m_4), and external chair (m_5) for BCG measurement. This model also contains seven pairs of spring (k) and damping (c) coefficients. These physical parameters vary among different individuals [54]. BCG transmission from internal blood vessels to the external body can be estimated as an encryption process due to non-linear effects [34]. The encrypted BCG signals are measurable by the accelerometer on the chair, laying the fundamental principle for CA in NF-Heart.

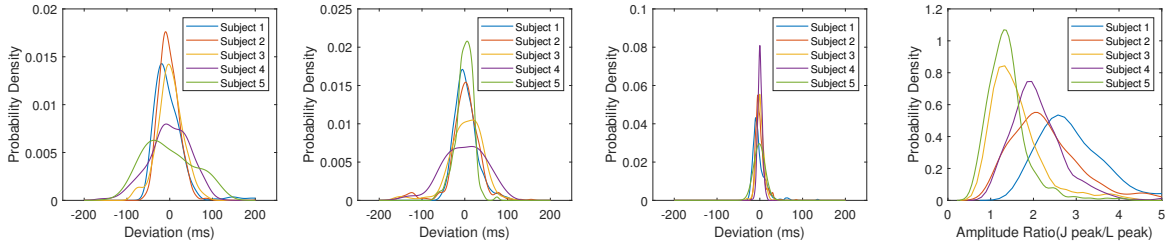

(a) Deviation of J-J interval (b) Deviation of cycle duration (c) Deviation of I-J interval (d) Amplitude ratio of J to L

Fig. 5. Characteristics of BCG signals.

2.3 Characteristics of BCG Signals

Three-dimensional deformation of the heart induces unique mechanical vibrations because the cardiac cycle states significantly differ in terms of volume, surface shape, and motion dynamics (i.e., displacement, velocity, and acceleration) of the heart [9]. It is nearly impossible for two individuals to have the same heart, vascular tree, and tissue characteristics [17]. The intra-subject variability of BCG data is low for a certain long period [58]. Therefore, the BCG data can serve as distinctive biometrics for each individual.

We conduct a pilot study on five subjects sitting on a prototype BCG chair (see Figure 3) and analyze their BCG signals. Figure 4(b) plots one-cycle BCG samples from two subjects. The signals are aligned with the I-wave. We can observe that the BCG patterns of the different subjects are distinct. For the same subject in Figure4(c), the BCG signals maintain consistency over time, although the respiratory motion causes a slight variation in the morphology.

Figure 5(a) depicts the probability density function (PDF) of the deviation in the time interval between two consecutive heartbeats, and Figure 5(b) depicts the PDF of deviation during one cardiac cycle. These two figures demonstrate the intrinsic HRV in BCG signals. In addition, we can also observe the variation of the amplitude ratio of the J-peak to L-peak from Figure 5(c). Sometimes the L-peak value will be larger than the J-peak value. Based on these observations, we can conclude that BCG signals vary in both amplitude and the timing of each peak. This makes signal segmentation and delineation rather challenging. Fortunately, we also observe that the deviation of the I–J interval is much smaller than that of the J–J interval. This indicates that BCG biometrics can be extracted based on the relationships between each fiducial point. (see Section 5.1).

3 OVERVIEW OF NF-HEART

3.1 System Overview

The system architecture of NF-Heart is shown in Figure 6. It comprises several major procedures that allowed us to build a secure, robust, and practical CA system using BCG biometrics.

The signal-processing pipeline first applies a bandpass filter to remove the high-frequency noise. Then, it leverages an instantaneous power-based segmentation to acquire discrete cardiac cycles.

MAs often occur at a high frequencies in BCG signals, which prevents the practical deployment of BCG-based applications. We first need to detect the time when MAs occur before removing it. Instead of using traditional methods that rely on matching designated BCG templates or analyzing temporal statistics separately, we design a Hidden Signal Quality Index (H-SQI) to accurately detect arbitrary types of MAs. Afterward, the detected MA will go through a two-stage MA-removal using the complete ensemble empirical mode decomposition with adaptive noise (CEEMDAN), and variable step-size least mean squares (VS-LMS) algorithms. The combination of CEEMDAN and VS-LMS facilitates adaptive MA-removal according to the signal characteristics.

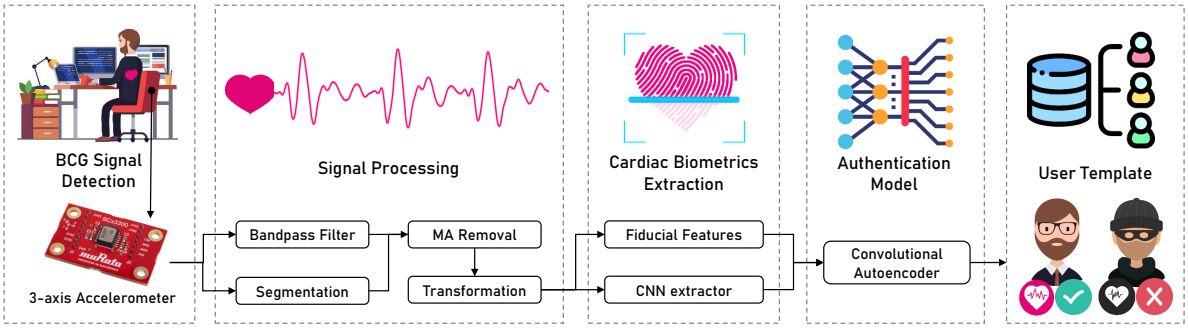

Fig. 6. System overview of NF-Heart.

The signal processing pipeline ends up with a transformation step that eliminates the uncertain effects of respiration, heart rate variability, and posture variation. The transformation process builds upon the elaborate BCG dynamic model with 14 Gaussian kernels. It can eliminate the effect of uncertainties while maintaining the local features in BCG signals. After signal processing, we obtain clean BCG signals.

The next step is to delineate BCG signals and extract user-specific features for authentication. Specifically, we present the first attempt to delineate seven fiducial points of BCG using a modified lightweight U-net architecture. We define 45 fiducial features for characterizing BCG signals. The user verification can be estimated as anomaly detection, where the biometric signals of attackers are anomalies. Thus, we adopt the unsupervised convolutional autoencoder (CAE) as our authentication model.

For a practical use case, a new user first needs to register their BCG biometrics in the system. The data collection time will last for 2 minutes. The collected data will be used to train a private CAE model after pre-processing. Afterward, if the users want to start a session, they will need to specify the identity (e.g., username) that they wants to log in with. Then, NF-Heart will continuously read the BCG biometrics as the input of CAE to verify the user's legitimacy.

3.2 Attack Model

In this section, we introduce three major attack scenarios that NF-Heart may be against.

3.2.1 Spoofing Attacks. A spoofing attack is one of the most typical attacks in our daily lives, which indicates when an imposter attempts to spoof the system with their cardiac biometrics and gain access to the system. There is a high risk of divulging confidential information even if only several consecutive heartbeat cycles of the imposter are erroneously authorized. To conduct a spoofing attack, the adversaries will sit on the chair with the NF-Heart authentication system directly and attempt to imitate a legitimate user's BCG biometrics by adjusting their cardiac motion in different ways, such as holding breath and doing exercise.

3.2.2 Random Attacks. NF-Heart collects BCG signals with an accelerometer. Therefore, the vibrational interference from the nearby environment may possibly be detected by the system. An attacker might attempt to forge the periodic signal using different means, including but not limited to periodic actions of finger taps, percussion with a hammer, and foot-stomping.

3.2.3 Replay Attacks. Nowadays, the leakage of biometric data is common. Thus, the cardiac pattern of legitimate users might be somehow obtained by imposters, which gives an opportunity to conduct a replay attack. A user authentication system (e.g., face recognition) is prone to suffer replay attacks if no liveness detection scheme is

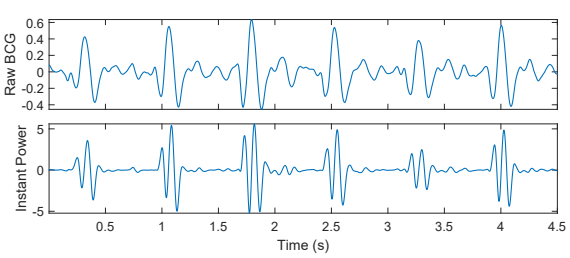

Fig. 7. Illustration of IP for heartbeat segmentation.

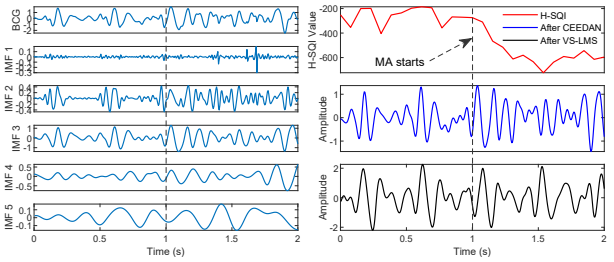

Fig. 8. Decomposed IMFs using CEEMDAN (left). The H-SQI values for MA detection. The results of MA removal.

performed. In our case, we assume that the adversaries have obtained the BCG biometrics of legitimate users. They can attach a vibrator on the chair to replay the original BCG signals for spoofing the NF-Heart system. Note that we do not consider the replay attacks that the adversary directly inputs the BCG signals into the on-device/on-cloud CAE model by hacking the inner data transmission pipeline in this paper.

4 SIGNAL PROCESSING

4.1 Bandpass Filtering

The BCG measurement is realized by attaching a three-axis accelerometer to the chair's back. The BCG sensor mainly records data from the torso section when a user is seated. There is no direct contact between the sensor and the user's skin. BCG signals manifest as ultra-low frequency and have a narrow bandwidth of 0.5 - 10 Hz [49]. Thus, we apply a third-order Butterworth bandpass filter within this bandwidth to remove high-frequency interference and low-frequency noise (e.g., baseline drift, DC components, and respiration). However, the morphology of BCG is influenced by lung volume [22], and distortions caused by breath motion, which are hard to completely reverse with a bandpass filter. Besides respiratory interference, it is unfortunate that the BCG signal bandwidth coincides with other interference sources, such as body movement. Therefore, a further MA detection and removal scheme will be discussed to enhance system performance.

4.2 Segmentation

An early stage of segmentation is indispensable, which prepares the discrete cardiac cycles for the execution of subsequent modules. To extract each heartbeat, we design an intuitive algorithm to locate the prominent J-peak. As shown in Figure 7, we observe that the N–H interval between two heartbeats is relatively smooth. Thus, we leverage the instantaneous power ($IP = Force \times Velocity$) to enhance this smoothness as:

$$IP = m_0 a(t) \cdot \int a(t) \tag{2}$$

where $a(t)$ consists of accelerometer readings and m_0 is the mass, which is set as a constant. Now we can get the location of the J-peak (Loc_J) through the local maximum IP. The typical length of a cardiac cycle is set as $[Loc_J - 0.3s, Loc_J + 0.5s]$.

4.3 Two-stage Motion Artifact Removal

In this section we present our two-stage MA-removal scheme for addressing the long-standing open issue regarding motion artifact effect.

4.3.1 Motion Artifact Detection. We first use a bandpass filter to remove filterable high-frequency noise ($> 10Hz$). Afterward, we focus on tackling any "unfilterable" noise superposed upon the BCG signals in the same frequency

band. From the perspective of noise duration in the time domain, we can classify the noise into two types. The first one is sudden noise, which is short and pulse-like. The causes of sudden noise could be subconscious posture changes or items falling on the ground. The second type is continuous noise, which could be caused by continuously typing on a keyboard during office work and swaying of the body to musical rhythms.

MA detection should accurately detect the time when an MA occurs. Targeted processing of detected noise segments instead of the whole time series can effectively reduce unnecessary computation overheads. Traditional methods for MA detection are based on calculating the correlation level between a template signal and current signal [67]. Another way is to set empirical thresholds of some statistics such as standard deviation, skewness, kurtosis, and so on [71]. However, there are many types of noise in real scenarios; correspondingly, the degree and duration of the influence of MAs on BCG morphology will vary case by case. Hence, it is difficult for traditional methods to cover different types of MAs.

To tackle different cardiac conditions and signal abnormalities, our idea is to proposed a comprehensive signal quality index (SQI) to evaluate each segment and judge whether the segment is a valid and high-fidelity BCG cycle or not. We attempt to measure seven temporal statistics, including the standard deviation, root mean square, kurtosis, skewness, impulse factor, clearance factor, and shape factor. However, it is hard to empirically constitute a uniform formula (i.e., SQI) with these statistics. Therefore, we resort to machine-learning techniques. Specifically, we leverage the Hidden Markov Model (HMM) [48] to acquire the SQI. HMM is a classic and effective algorithm for speech detection. The key insight here is that HMM was effective in speech detection in the earlier days of speech recognition. It can effectively recognize the same word pronounced by different people. Therefore, we can take the BCG cycle that varies from person to person as a "word". We separately trained two HMM models using raw BCG signals and seven statistics. We can finally get the Hidden Signal Quality Index (H-SQI) by summing up the output probability values of two HMM model (two HMM model provide better outcome). The H-SQI result of a template BCG is shown in Figure 8.

We use the manually examined BCG segments from different users to train a lightweight HMM template. The Baum–Welch algorithm [66] is used to estimate model parameters. Segments that have low H-SQIs will be fed into the next step for MA removal.

4.3.2 Motion Artifact Removal. There are two schemes for MA removal after MAs are detected. The first one is to delete the interfered part directly. This scheme is simple but crude. It will make the heartbeat signal discontinuous and result in the lose of much sequential information. In addition, it will degrade the system's performance if multiple cycles are needed for user authentication. In some extreme cases with continuous interference, the system may receive zero cycle and fail to work.

Another scheme is to reconstruct a noisy waveform back to a clean one. This is challenging because the collected BCG signals are aliased with a lot of interference in the same frequency band. A common solution is to perform interpolation based on the information of clean adjacent cycles to replace the contaminated part. However, this is not applicable for continuous MAs.

Therefore, we design a two-stage MA-removal scheme for both sudden and continuous MAs. The first stage decomposes the raw signal into multiple components and eliminates components that distort signal's morphology. Through linear combination, the remaining components will form a reconstructed intermediate signal fed into an adaptive filter for deeper noise cancellation.

The first stage with CEEMD. The BCG signals aliased with various random noise are nonlinear and non-stationary signals. Decomposition based on wavelet transform is very suitable for such kinds of signals. However, wavelet transform requires choosing a suitable wavelet basis function, which indicates that the wavelet-based method cannot perform optimal decomposition according to the structural characteristics of each person's BCG signals. Therefore, we adopt the empirical mode decomposition (EMD) method, which is also designed for processing nonlinear and non-stationary time-series, for the first stage of MA removal.

EMD can perform adaptive signal decomposition based on the time-scale characteristics of the signal itself. Compared with wavelet-based methods, it does not need to determine a basis function in advance. It can decompose a complicated signal into a finite number of intrinsic mode functions (IMFs) as shown in Figure 8. The decomposed IMF components are instantaneous frequency components, which contain the local characteristics of the original signal at different time scales.

Specifically, we adopt CEEMDAN algorithm [60], which is an improved version of EMD [19]. Compared to EMD, CEEMDAN addresses the mode-mixing problem in EMD by adding random white noise to the raw signal, and it can use a fewer number of sifting iterations to decompose signals into IMFs with less noise for reconstruction.

CEEMDAN iterates upon the EMD approach, where the BCG data $x(t)$ is decomposed into several IMFs ($k = 1, 2, \ldots, K$) and residual r_K:

$$x(t) = \sum_{k=1}^{K} IMF_k + r_K \tag{3}$$

Each IMF is subject to the following two constraints: 1) the number of extrema and the number of zero-crossings must equal or differ at most by one; 2)the mean value of the upper and lower envelopes defined by the extrema is zero at any point. The procedure of extracting an IMF is called sifting. We refer the readers to [19] for more details about sifting.

Now we define the operator $E_j(\cdot)$, which produces the j-th mode calculated by EMD and let ε_k be coefficients that allow SNR selection at each stage. CEEMDAN algorithm can be described as following steps:

(1) Generate $x^i(t) = x(t) + \varepsilon_0 n^i(t), i = 1, 2, \ldots, I$, where $n^i(t)$ are white Gaussian noise.

(2) Decompose $x^i(t)$ with EMD, finding the modes IMF_k^i, where $k = 1, 2, \ldots, K$.

(3) At the first stage ($k = 1$), the first mode $\widetilde{IMF_1}$ and first residual r_1 are computed as

$$\begin{cases} \widetilde{IMF_1} = \frac{1}{I} \sum_{i=1}^{I} IMF_1^i \\ r_1 = x(t) - \widetilde{IMF_1} \end{cases} \tag{4}$$

(4) The first residual is forwarded to the next stage. The second mode can be obtained by decomposing realizations $r_1 + \varepsilon_1 E_1(n^i(t))$. Formally, the second IMF is defined as:

$$\widetilde{IMF_2} = \frac{1}{I} \sum_{i=1}^{I} E_1 \left(r_1 + \varepsilon_1 E_1(n^i(t)) \right) \tag{5}$$

(5) For $k = 2, \ldots, K$, we have the k-th IMF and residual:

$$\begin{cases} \widetilde{IMF_k} = \frac{1}{I} \sum_{i=1}^{I} E_1(r_{k-1} + \varepsilon_{k-1} E_{k-1}(n^i(t))) \\ r_k = r_{k-1} - \widetilde{IMF_k} \end{cases} \tag{6}$$

The decomposition stops until the obtained K-th residual is no longer feasible to be decomposed. The decomposed IMFs follow the descending order of the frequency (i.e., the frequency of IMF_1 is higher than that of IMF_2). The IMFs of higher frequencies tend to be noise or MAs. A correlation-based IMF selection metric [68] is applied to remove the undesired IMFs and form a final IMF set $\mathcal{S}$ for reconstruction. Therefore, the reconstructed BCG is expressed as:

$$\tilde{x}(t) = \sum_{k \in \mathcal{S}} IMF_k + r_K \tag{7}$$

The second stage with VS-LMS. Unfortunately, the pseudo-periodicity of BCG signals makes it impossible to completely eliminate MAs with only CEEMD. There are still some residual MA components in the decomposed IMFs. We need to perform adaptive filtering to further optimize the quality of the BCG signals.

Adaptive filtering allows for the automatic adjustment of filtering parameters to achieve optimal performance according to the input signal's actual situation and structural characteristics. The least mean square (LMS) adaptive filter is one of the most prevalently used adaptive filters. It has a simple structure, stable performance, and low computational complexity. But the main disadvantage of LMS is that its convergence speed is relatively slow. Therefore, we apply the variable step-size least mean squares (VS-LMS) [31] for the second stage of MA removal to get a faster convergence speed and lower steady-state error. The reconstructed BCG signals can be seen in Figure 8.

4.4 Transformation

Signal variability is another critical challenge for CA using heartbeat biometrics. For BCG signals, in addition to being affected by intrinsic HRV, the signal morphology will also be affected by other uncertainties such as different respiration patterns, sitting postures, and emotional states. It is non-trivial to design a method that can eliminate these multiple uncertainties while retaining the user-specific characteristics of BCG signals.

To this end, we adopted and modified the dynamical ECG model of [39], thus proposing the BCG dynamical model for transformation as follows:

$$\begin{cases} \dot{x} = \gamma x - \omega y \\ \dot{y} = \gamma x - \omega y \\ \dot{z} = -\sum\limits_{i \in \{H,I,J,K,L,M,N\}} a_i \Delta\theta_i \exp(-\dfrac{\Delta\theta_i^2}{2b_i^2}) - (z - z_0) \end{cases} \tag{8}$$

where $\gamma = 1 - \sqrt{x^2 + y^2}$ and ω is the angular velocity, which is related to the beat-to-beat heart rate as $\omega = 2\pi f_1$. $\Delta\theta_i = (\theta - \theta_i) \bmod 2\pi$, where $\theta = \arctan(y/x)$. The BCG signals' H-, I-, J-, K-, L-, N-, M-waves are transformed with a Gaussian kernel. The kernel parameters contain θ_i, a_i, and b_i, referring to the center position, peak amplitude, and width of each wave, respectively. The baseline wander of a BCG caused by respiration is modeled with $z_0 = A\sin(2\pi f_2 t)$, where f_2 is the respiratory frequency. We can remove the respiration effect by neglecting the z_0 term. The transformation of BCG signals is finished by integrating the $\dot{z}$ equation using the fourth-order Runge–Kutta method [59] with a fixed time step $\Delta t = 1/f_s$ where f_s is the sampling frequency. To address the intrinsic asymmetry problem [10] of BCG signals, we assign two Gaussian kernels to each wave (14 kernels in total). The kernel-parameters fitting can be considered as a minimization problem between the raw BCG signals $\hat{x}(t)$ and $z(t)$, that is:

$$\min_{\theta_i, a_i, b_i} ||x(t) - z(t)||_2^2 \tag{9}$$

over all seven i. Equation (9) can be easily solved using multi-dimensional gradient descent in parameter space [42].

5 FEATURE EXTRACTION AND USER AUTHENTICATION MODEL

5.1 Definition of Fiducial Features

Robust heart biometrics-based authentication highly relies on extracting unique and invariant features. The fiducial-point method is one of the most effective ways to achieve this. The fiducial points are indicators of each cardiac event and have physiological meanings in clinical practice. The fiducial features can provide intrinsic geometrical information of the heart and reflect 3D deformation when the heart is pumping. Here, we present

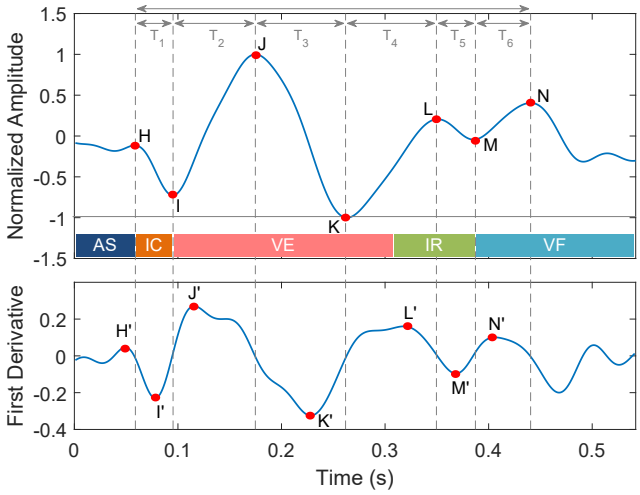

Fig. 9. Definition of fiducial points (H to N). AS, IC, VE, IR, and VF are cardiac events detailed in Appendix.

Table 1. The definition of fiducial features based on fiducial-point delineation.

Feature Type	Feature Name	Description
Time Interval	DU=T(H, N), T(H, I), T(I, J), T(J, K), T(K, L), T(L, M), T(M, N) T(H', I'), T(I', J'), T(J', K'), T(K', L'), T(L', M'), T(M', N')	Time interval between each two consecutive fiducial points
Time Ratio	T(H, I)/DU, T(I, J)/DU, T(J, K)/DU, T(K, L)/DU, T(L, M)/DU, T(M, N)/DU	Ratios of section to whole cycle
Extremum	A(H), A(I), A(J), A(K), A(L), A(M), A(N) A(H'), A(I'), A(J'), A(K'), A(L'), A(M'), A(N')	Peak values of fiducial points
Displacement	|A(H)-A(I)|, |A(I)-A(J)|, |A(J)-A(K)|, |A(K)-A(L)|, |A(L)-A(M)|, |A(M)-A(N)|	Differences between Y-axis of points
Area Under Curve	AUC(H, I), AUC(I, J), AUC(J, K), AUC(K, L), AUC(L, M), AUC(M,N)	Area enclosed by $S_{bcg}(a, b)$ and $Y = min(S_{bcg})$

the first exploration of extracting 45 BCG geometrical features based on the seven fiducial points, i.e., peaks H to N, as shown in Figure 9. Note that we also extract the corresponding fiducial points on the first derivative of BCG signals, i.e., peaks H' to N'. We neglect G-peak because it often disappears.

As described in Table 1, we define five types of fiducial features, including the time interval, time ratio, extremum, displacement, and area under curve (AUC). As shown in Figure 9, we define the duration (DU) of one-cycle BCG signals (S_{bcg}) as the time interval between the H and N peak. One cycle is divided into 6 sections depending on the timing of the fiducial points. Particularly, the AUC refers to the area enclosed by a specific section of S_{bcg} and the horizontal line $Y = min(S_{bcg})$.

5.2 BCG Delineation

Previous works for BCG delineation mainly focused on locating the most prominent J-peak using an envelope analysis [43] and correlation-based template matching [52]. The purpose of such kind of delineation is to measure the heart rate. It seems to be easier to label all the other fiducial points after determining the J-peak. [1] assumed that the other fiducial points have a relatively fixed relationship with the J-peak and will present in a certain empirical search-range from J-peak's location. However, this assumption is contrary to the actual situation, making this method error-prone. In addition, an adaptive algorithm for deciding the search-range remains to be designed to address the individual's variability.

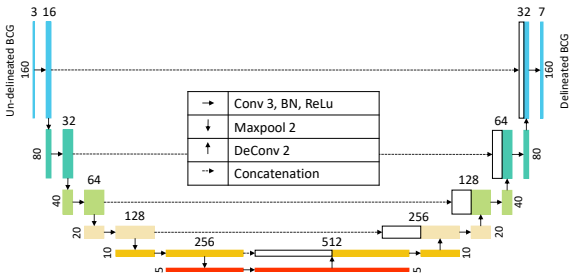

Fig. 10. U-net architecture for BCG delineation.

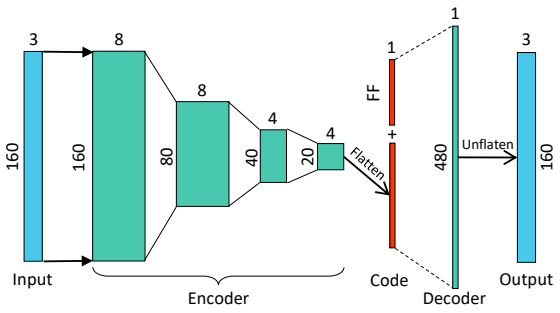

Fig. 11. Convolutional autoencoder framework.

To achieve the accurate delineation of BCG signals, we take advantage of deep-learning techniques to automatically label fiducial points. Specifically, NF-Heart refers to a deep convolutional neural network (CNN)—the U-net architecture [50], which has been widely used in the precise segmentation of biomedical images. Compared to the original U-net architecture, we modify and refine it by removing the convolution layer in the middle of each level so that it can precisely locate fiducial points on one-dimensional BCG signals with fewer parameters.

The modified U-net architecture for BCG delineation is shown in Figure 10. It consists of contracting layers on the left side and expansive layers on the right side. Each rectangle is a multi-channel feature map whose height is the number of sample points and width is the number of channels. Particularly, the white rectangle is a copy of the feature map from the left side to the right side. Three-channel (3-axis) BCG signals with 160 sample points are fed into the contracting layers. Each floor follows the typical architecture of one CNN with zero-padding convolution, batch normalization (BN), and a rectified linear unit (ReLU). Then, a max-pooling operation with stride 2 is used for downsampling into the next floor. The expansive layers account for the upsampling of the feature map with deconvolution that halves the number of channels. The output feature map from the left side is concatenated to the right side of the same floor. NF-Heart aims to label seven fiducial points, i.e., H peak to N peak. Hence, the output layer has seven channels where each channel vector indicates the probability of each sample point as a corresponding fiducial point. The cross-entropy loss function is used for training the network parameters. In summary, the input BCG segment is forward propagated through the U-net architecture, and NF-Heart can automatically label the seven fiducial points based on the output probabilities. In the end, the corresponding fiducial features is extracted.

5.3 User Authentication Model

We adopt the CAE [38] as the user authentication model. The intuition behind this is that we can consider the verification process as noise detection, where a legitimate user's BCG signals are valid, but that of an attacker is noise.

A CAE consists of an encoder and decoder, as shown in Figure 11(c). The encoder is responsible for encoding the input BCG signals by mapping it into a lower-dimensional latent space using four levels of convolution. We aggregate the latent features with pre-extracted fiducial features. Then, the aggregated features are utilized for decoding. The decoder will reconstruct the original input BCG signals using one layer of fully connected neural network. The input BCG of attackers cannot be reconstructed using the trained CAE model of legitimate users. The parameters of CAE are trained by minimizing the mean square error loss function between the input BCG and reconstructed BCG.

There are two benefits of using CAE: 1) The CAE is unsupervised learning; thus, no prior knowledge of the attacker is required to train the model parameters. 2) The convolution layer can further extract some other useful features from the raw 3-channel BCG signals. Note that we do not extract frequency-domain features because of the ultra-low frequency bandwidth of BCG signals.

6 EVALUATION

6.1 Experimental Setup

6.1.1 Implementation. We prototype NF-Heart with BCG measurement using a Murata 3-axis accelerometer SCA3300-D01. We deploy the sensor node on the chair's back to collect the BCG signals of the seated users, as shown in Figure 3. The sampling frequency of the BCG sensor is set to 1000 Hz. The BCG readings are transmitted to a laptop through the wire for further signal processing and user authentication.

6.1.2 Cardiac Data Collection. We recruit 105 healthy subjects (32 of them are females) with an age range of 18 to 57 from our university. We construct a main dataset with 105 subjects' BCG samples to demonstrate the baseline performance of NF-Heart. The subjects involved in the main dataset are asked to sit still and recline against the chair's back for 5 minutes. In addition, we further ask 10 subjects to evaluate the system's robustness and the data of which form several separate sub-datasets. The different experimental conditions of sub-datasets will be specified in the corresponding section. Note that the conducted experiments conform to the IRB protocol (PN-2020-040) of our university.

6.1.3 Authentication Strategy. We alternately designated each subject as a legitimate user, and the remaining $N-1$ subjects take the role of an attacker to test the system model (N = 105).

6.2 Evaluation Metrics

To evaluate the system, we use several evaluation metrics including the balanced accuracy (BAC), receiver operating characteristic (ROC), area under curve (AUC), and equal error rate (EER).

6.2.1 Accuracy Metrics. The distribution of positive and negative samples is unbalanced in our case, so we adapt the BAC to evaluate the system accuracy. BAC is not sensitive to the class distribution and can prevent misleading accuracy measurements. The BAC equally combines the true positive rate (TPR) and true negative rate (TNR), which is defined as:

$$BAC = \frac{TPR + TNR}{2} = \frac{0.5 \times TP}{TP + FN} + \frac{0.5 \times TN}{TN + FP} \tag{10}$$

where TP, TN, FP, and FN refer to the true positive, true negative, false positive, and false negative, respectively. $TP + FN$ and $TN + FP$ are the amounts of positive samples and negative samples, respectively.

6.2.2 ROC Curve. An ROC curve is obtained by plotting the TPR against the false positive rate (FPR) under different loss thresholds. TPR indicates the percentage of samples that are correctly identified as legitimate samples in all legitimate test samples, while FPR is defined as the percentage of samples that are wrongly identified as legitimate samples in attack samples. Equal error rate (EER) is the point where the FPR is equal to the $1 - TPR$ (i.e., false negative rate).

6.3 Verification Accuracy

6.3.1 Impact of Training Set Size. New users must first record their heartprint into NF-Heart to initialize their own authentication model. In this experiment, we explore the impact of different heartprint collection time (HCT), i.e., different training set sizes, on verification performance. Specifically, we increase the HCT from 0.5 to 3.5 minutes with a step size of 0.5 minutes. In order to collect as many samples as possible, a sliding window

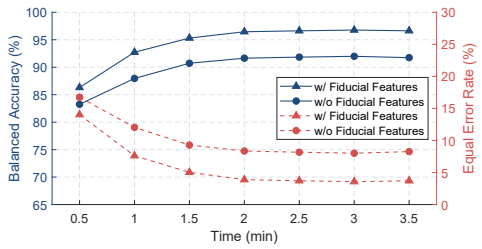

Fig. 12. Impact of the HCT for model initialization.

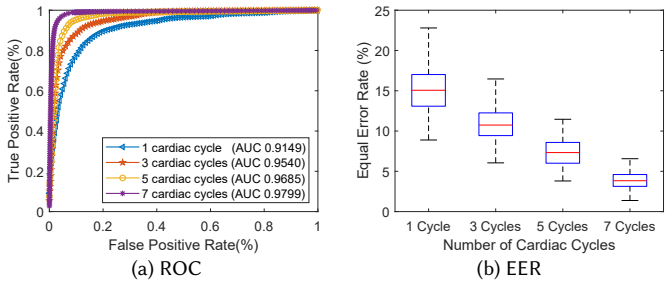

(a) ROC (b) EER

Fig. 13. ROC curves and EER with different number of cardiac cycles.

with a stride of 1 cycle is used to collect seven consecutive cardiac cycles as training samples. Figure 12 shows the effect of different HCT on the accuracy of verifying legitimate users. It can be seen that when the HCT is 0.5 minutes, NF-Heart can provide a high verification accuracy of about 86.30%. The BAC then rises to above 96.45% on average when HCT extends to 2 minutes. A further extension of HCT can only provide a marginal improvement in accuracy. Therefore, the optimal HCG should be 2 minutes, and we adopt this setting for the following experiments.

6.3.2 Impact of Feature Subset. We also validate the effectiveness of the fiducial features, where the results are shown in Figure 12. Obviously, the fiducial features capture geometric deformation of the heart well and yield a higher verification accuracy and lower EER compared to using only raw signals. On average, BAC improves by 4.56%, and EER declines by 4.23% when HCT equals 2 minutes.

6.3.3 Impact of Cardiac Cycles Number. Another important parameter that affects authentication performance is the number of cardiac cycles used for authentication. Theoretically, extra heartbeat cycles can provide more biometric information to achieve higher verification accuracy. To validate this assumption, we evaluate our system using different segment lengths. Figure 13 (b) depicts the ROC curves for different numbers of cardiac cycles. The AUC for each curve is 0.9149, 0.9540, 0.9685 and 0.9799 for segments with 1 cycle, 3 cycles, 5 cycles, and 7 cycles, respectively. In addition, as shown in Figure 13 (c), the median EER is 15.06%, 10.74%, 7.33% and 3.83% for 1 cycle, 3 cycles, 5 cycles, and 7 cycles, respectively.

6.4 Security Analysis

In this section, we investigate the vulnerability of NF-Heart and validate that our proposed CA scheme is safe and secure under the three types of attacks described in Section 3.1.

6.4.1 Spoofing Attacks. To simulate the spoofing attacks, we feed the adversary samples to test the trained legitimate user's model. Each legitimate model will be attacked by 104 patterns of BCG biometrics. Note that we have presented the comprehensive results for spoofing attacks in the previous section. In summary, NF-hear achieves a median false positive rate (FPR) of 3.83% when the heartprint collection time is 2 minutes and the segment length is seven cardiac cycles. This indicates that the BCG biometrics is hard to be imitated by adversaries, and NF-Heart can resist the spoofing attack.

6.4.2 Random Attacks. For a live individual, his/her cardiac activity is non-volitional, and their heart-based biometrics are hard to hide once they sit on the chair equipped with the NF-Heart system. Suppose that no one is sitting on the chair: NF-Heart may still detect a periodic signal and activate the authentication pipeline since we use the energy-based algorithm for segmentation. Therefore, we perform a random attack by generating periodic vibrations produced by finger taps, hammer percussion, and foot stomps. Each action lasts for 3 minutes, and the execution frequency is 70 bpm synchronized with a metronome. Then the generated signals are used as test

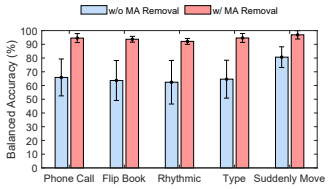

(a) BAC

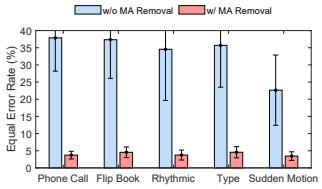

(a) EER

Fig. 14. The effectiveness of the two-stage MA removal.

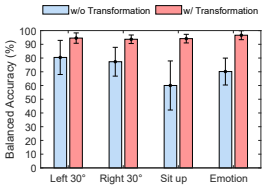

(a) BAC

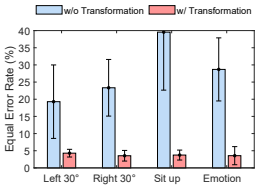

(b) EER

Fig. 15. The effectiveness of transformation.

samples to attack every subject in the main dataset. The results show that none of the random attack samples can be successfully authenticated.

6.4.3 Replay Attacks. Replay attacks are the most significant threat to biometrics-based authentication systems. It is common that the users' biometric tokens (e.g., face and fingerprint) to be stolen or leaked by a third party. Although heartbeat biometrics are more complex, implicit, and dynamic, thus making them harder to counterfeit, we have to validate that NF-Heart is not vulnerable to replay attacks. Specifically, we use a vibration microphone to replay each subject's original BCG signals and the accelerometer sensor to collect the replayed BCG signals, which are then added to the test samples of the corresponding subject. The result shows that all replay attacks are rejected by NF-heart. The rationale of this result can be revealed in Figure 2, where the BCG signals are modulated by the individual's unique body (i.e., unique vascular structure and spring-mass-damper coefficient). A simple replay of raw BCG signals can not achieve the proper harmony and coupling of the system. Thus, the received accelerometer readings are actually distorted to varying degrees. This is like the near-field BCG biometrics feature with a liveness detection function intrinsically.

6.5 Robustness

In this section, we evaluate the system's robustness under different practical situations and validate the effectiveness of the proposed signal-processing pipeline. A long-term study is also conducted to show the temporal stability of NF-Heart.

6.5.1 Motion Artifacts. All subjects are first asked to sit still for 5 minutes to collect baseline BCG samples. Then, they are asked to perform five rounds of MA collection, including making a phone call, flipping a book, swaying to the music, typing on a keyboard, and sudden body motions. Each round lasts for 2 minutes. The first four rounds are continuous MAs performed for 15 s after every 15-second static rest. As a result, one out of two minutes of the BCG signals interfere with the continuous MAs. Particularly, a sudden body motion is performed once every 10 s. Figure 14 shows the impact of different MAs and the effectiveness of our MA-removal scheme. Comparing to the baseline result, the MA removal algorithm increases the BAC by 26.93% and reduces the EER by 29.64%on average. Thus, the system performance can be significantly improved after enabling MA removal.

6.5.2 User State. In practical usage, users undergo different sitting postures and emotional states, resulting in different heart rates and BCG morphologies. In this experiment, we investigate the impact of different user states on system performance and validate the efficacy of using the transformation technique to eliminate negative effects. Specifically, the subjects are asked to perform other three sitting postures (i.e., turn left 30°, turn right 30°, and sit up without reclining) that are different from the baseline posture (i.e., reclining on the chair). To simulate different emotional states, the subjects are asked to raise their heart rate to over 120 bpm through exercise before data collection. Their heart rate will gradually restore to normal level (50-80 bpm) during the data collection process. Each type of state lasts for 2 minutes. In Figure 15, the varying user states degrade the system

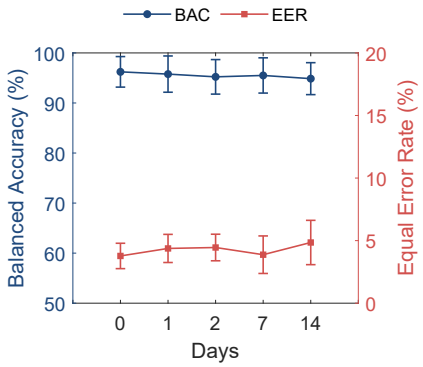

Fig. 16. Temporal stability over 14 days.

performance to different degrees as expected, where the BAC declines by 22.76%, and EER rises by 23.93% on average. Fortunately, the system performance can be restored by applying the transformation to the BCG signals.

6.5.3 Temporal Stability. An authentication system of high availability should maintain long-term performance. To validate this critical ability of NF-Heart, we conduct an experiment spanning 14 days. Ten subjects are asked to collect their BCG signals for testing on the same day (where data from day 0 are used as baseline), after 1 day, 2 days, 7 days, and 14 days. Figure 16 demonstrates how the BAC and EER of NF-Heart change over time. Overall, the BAC is higher than 94.50%, and EER is lower than 4.90%. On the fourteenth day, the BAC and EER have no large variation, achieving 94.86% and 4.85%, respectively. Thus, we can conclude that the performance of NF-Heart has no significant degradation after a 14-day period and the BCG biometrics are robust against temporal changes. However, the BCG biometrics may vary over a longer period than 14 days, resulting in performance degradation. In addition, the body status changes due to some diseases may also introduce variance to the original BCG morphology. We would suggest a calibration process with moderate frequency (e.g., 14 days) in practical use.

7 RELATED WORK

Heartbeat-based identification: Heartbeats are measurable vital signs in all living individuals. The deformation of the heart is unique across different subjects, and the heartbeat signals are hard to hide and forge, making heart-based biometrics an attractive approach for identifying users. ECG sensors are widely deployed in the heart-based identification systems to capture heart bio-signals [44]. Zhao et al. [72] propose an ECG-based identification system using ensemble empirical mode decomposition. Heartbeat features are extracted by a Welch spectral analysis after the signal decomposition into multiple intrinsic mode functions. Heart-based biometrics are also used in mobile devices for user identification. Wang et al. [63] attach the smartphone to the chest of users to collect the seismocardiogram (SCG) signals using the built-in accelerometer. SCG signals refer to the vibrational response of the chest to the heart. The system authenticates users based on the correlation of SCG features extracted using discrete wavelet transform (DWT). CardioCam [37] captures cardiac biometrics from reflected lights when pressing a fingertip on the camera of a mobile phone.

For one-pass BCG authentication, Guo et al. [15] validate the feasibility of identifying individuals by analyzing the correlation between BCG signals collected with three S-beam load-cell sensors. The system performance is further improved by applying recurrent neural networks [69]. Hebert et al. [18] collect BCG signals using the inertial measurement unit (IMU) on a smart eyewear device for user authentication. In [23], the authors customize a glass-made floor tile in the kitchen and bathroom and embed four load cells inside the tile to collect

Table 2. Comparison of cardiac biometrics-based user authentication studies.

Work	Biometrics	Sensing Modality	Input Features	Methods	Subjects	Performance	CA	MA Tolerant
Guo et al. [15]	BCG	Three load-cell sensors on chair	raw BCG	Pearson Correlation	25	96% accuracy	✖	✖
Zhang et al. [69]	BCG	Three load-cell sensors on chair	raw BCG	LSTM	91	97.8% accuracy, 0.9% EER	✖	✖
Herbert et al. [18]	BCG	Accelerometer & gyroscope in smart Eyewear	raw BCG	CNN	12	3.5% EER	✖	✖
Javaid et al. [23]	BCG	Four load-cell sensors below glass tile	Discrete cosine transform	Linear Discriminant	56	96.15% accuracy	✖	✖
Camara et al. [7]	ECG	ECG electrodes	Walsh-Hadamard Transform	KNN-DNN	10	84.8% accuracy	✔	✖
Trueheart [71]	PPG	Wrist-worn PPG	5 Fiducial Features	Gradient Boost Tree	20	90.65% accuracy	✔	✔
PPGPass [8]	PPG	Wrist-worn PPG	40 Fiducial Features	Random Forest	7	95.3% F1 score	✔	✔
CardiacScan [36]	Cardiac motion	DC-coupled continuous-wave radar	8 Fiducial Features	SVM+DTW	78	98.61% BAC, 4.42% EER	✔	✖
NF-Heart	BCG	Accelerometer on chair back	raw BCG+ 45 Fiducial Features	Autoencoder	105	96.45% BAC, 3.83% EER	✔	✔

BCG signals. The proposed system calculated the discrete cosine transform (DCT) of the BCG sequence as features and identified samples with a linear discriminant (LD) classifier. In Table 2, we compare NF-Heart with existing BCG-based user authentication studies. On the other hand, we design a smart chair with a lightweight accelerometer for continuous user authentication. For the first time, we extract 45 fiducial features of BCG biometrics and tackle many practical interferences (e.g., motion artifacts), enhancing the system's usability and robustness.

Continuous user authentication: Traditional user authentication methods, such as password, grid pattern, fingerprint, iris scanning, and facial recognition identify the user only once at the very beginning, which is prone to be impersonated by attackers. In order to reduce the chance of impersonation, CA has been proposed to recheck the user's identity with a high frequency and distinguish between authorized users and impostors. Therefore, CA goes a step forward, strengthening system security and user safety. The proposed CA methods can be categorized into two main classes, namely, behavioral-based and physiological-based. Behavioral biometrics-based CA systems leverage the gait [65], gaze [56, 70], screen-touching [2, 13], hand gestures [55, 62], and keystroke [47, 51] dynamics to characterize users. These methods require the intensive involvement of users to perform specific actions for CA, which is inconvenient and limited to only a few application scenarios.

In Table 2, we compare different cardiac biometrics-based CA schemes. Carmara et al. [7] regarded the ECG signals as a continuous data stream and applied data stream mining (DSM) to explore bio-signals for CA. TrueHeart [71] and PPGPass [8] design low-cost CA schemes by exploiting the pulse bio-signals from PPG sensors. However, ECG-based and PPG-based systems are typically wearable devices and demand the user to make direct contact with the sensors, making the authentication procedure user-unfriendly. In contrast, RF-based systems can perform CA in a contactless manner. Cardiac Scan [36] employs a DC-coupled continuous-wave radar to capture high-fidelity heartbeat motion and extracts eight fiducial-based descriptors for real-time CA. However, RF-based systems are sensitive to the environmental variation and device settings (e.g., the angle and the distance of the device to the target). Compared to RF-based methods, NF-Heart not only provide a non-contact and unobtrusive scheme for CA but also has higher resilience to environmental changes and interference.

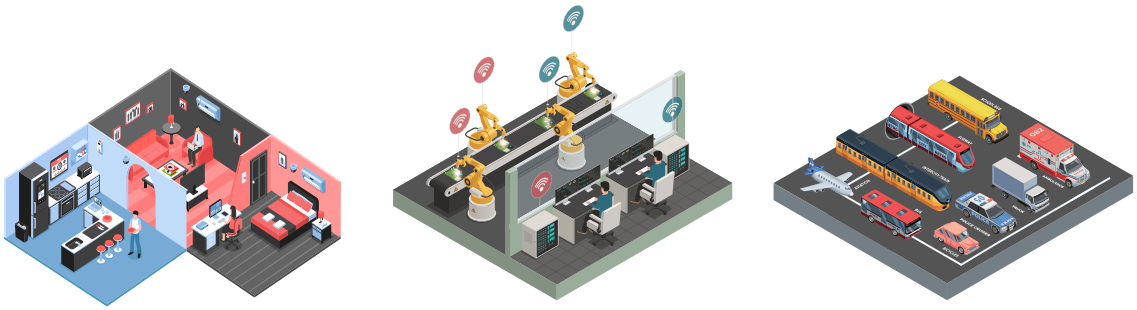

(a) Home (b) Factory (b) Transportation

Fig. 17. The illustration of more application scenarios.

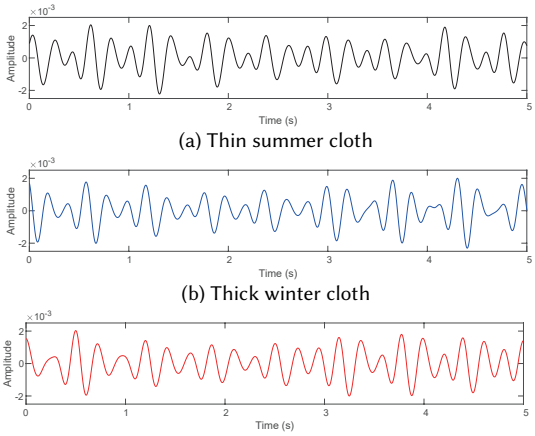

(a) Thin summer cloth

(b) Thick winter cloth

(b) Cushion padding

Fig. 18. The magnitude and morphology of BCG are consistent even with thicker padding between the user and the chair.

8 DISCUSSION

8.1 Extensive Application Scenarios

In fact, the practical deployment of NF-Heart can facilitate many other valuable applications, as shown in Figure 17. We envision that NF-Heart will include but not limited to the following application scenarios: 1) In the home environment, NF-Heart can dynamically adapt the ambient temperature, humidity, lighting conditions, music preferences, and TV preferences according to the family members' sitting locations. 2) In the workplace, NF-Heart can visualize the distribution of personnel and better manage energy use. 3) Furthermore, NF-Heart can ensure the safety of company assets. For specific equipment, it can only be operated or remote-controlled by authorized users. 4) For transportation, NF-heart can guarantee the legitimacy of drivers and avoid theft or hijack.

8.2 Failure Cases

In Section 6.5.1, we verify that NF-heart is resilient to MAs caused by body movement in daily work. However, what is the upper tolerance for interference? Is there any extreme case that may cause authentication failures, such as wearing heavy clothes, construction, or transportation? To answer these questions, we conduct several pilot experiments under different cases and plot the representative results in Figure 18 and Figure 19. The BCG biometrics remain the same whether wearing different thicknesses of clothing or placing a 5 cm-thick seat cushion.

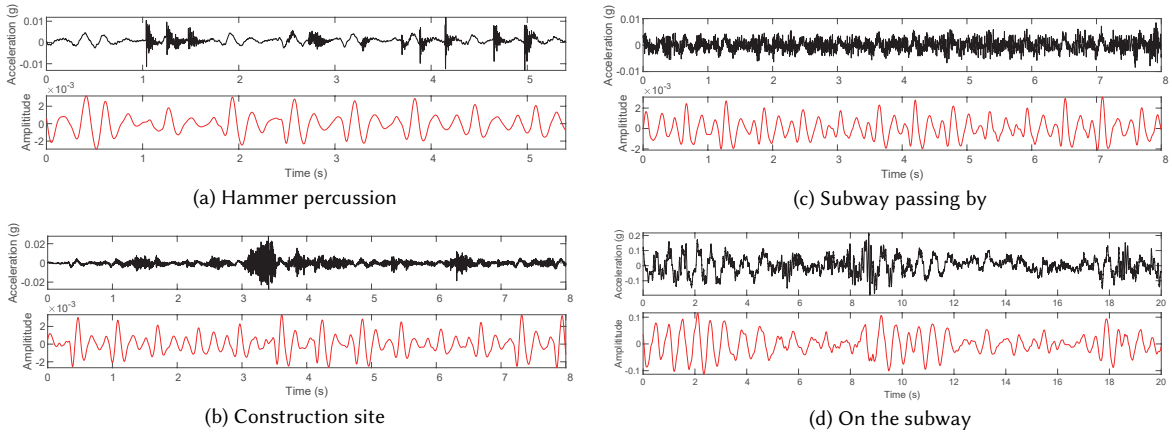

(a) Hammer percussion (c) Subway passing by

(b) Construction site (d) On the subway

Fig. 19. Signal recovery results under different levels of impulse or continuous noise. The black lines indicate raw acceleration reading, while the red lines indicate the corresponding recovered BCG biometrics.

The reason is that the BCG signals are caused by the gravity changes of the human body, and the clothing or padding will not weaken its amplitude or change its morphology. In Figure 19(a)–(c), we can observe that the raw acceleration readings suffer huge environmental interference. NF-Heart can restore the BCG biometrics well, no matter suffering impulse or continuous noise. However, the BCG biometrics is totally corrupted and can not be restored when the system is deployed on the subway. The interference magnitude (as high as 0.2 g) is ten times larger than other cases (e.g., 0.02 g for the construction site). This indicates that our current solution can not support CA on transportation. However, the authors in [21] successfully filter the transportation interference from BCG readings by using a seismic sensor as a noise reference. In the future, we may improve our interference cancellation ability by introducing extra noise reference sensors into the system and considering a more delicate algorithm design.

8.3 Privacy Concerns

Cardiac biometrics-based authentication systems bring new privacy threats to users, where the adversary can infer sensitive health information if they acquire the raw BCG waveform. Therefore, it is important to consider privacy protection in the authentication protocol. In general, a CA system can be deployed on cloud servers or edge devices. Several cryptography technologies, such as fuzzy commitment [25], fuzzy extractors [11], and fuzzy vault schemes [24], can be applied for privacy protection on authentication servers. On the other hand, a large amount of authentication protocol is proposed to encrypt sensitive health-related data on edge devices before sending it to cloud servers. Homomorphic encryption [14, 40, 41] can encrypt the biometrics on edge devices and allows computation on encrypted data to preserve confidentiality during processing on cloud servers. Cancelable biometrics approaches such as random projection [64], hashing [33], and salting [4] are introduced to solve privacy concerns for biometrics. Its core idea is to convert the raw biometrics template into a transformed one, where the adversary can not reverse the transformation process to get the original biometrics. In this paper, we mainly focus on proposing an advanced biometrics-based CA system while not considering the privacy protocol at the same time. We would like to incorporate the above-mentioned schemes into NF-Heart in the future.

9 CONCLUSION

Existing cardiac biometrics-based continuous authentication is unsatisfactory in many aspects, leaving much effort to be done for deploying in the wild. In this paper, we propose NF-Heart to fill the gap of near-field

non-contact CA using BCG biometrics. NF-heart can serve as a secure protector for organizations with a work-from-home policy. It can also combine with other schemes to perform multi-factor authentication for remote workforces. Compared to SOTA ECG or PPG-based CA scheme, NF-Heart does not require wearables or direct contact with sensor nodes. The fundamental principle of NF-Heart is to extract the unique biometric features of BCG signals measured from a chair where the user is sitting. The authentication of NF-Heart is unobtrusive, secure, robust, and user-friendly. The evaluation results validate that NF-Heart can function well under practical scenarios with arbitrary MAs, respiration effects, HRV, and posture variation.

ACKNOWLEDGMENTS

This research is supported in part by Guangdong Provincial Key Lab of Integrated Communication, Sensing and Computation for Ubiquitous Internet of Things, China NSFC Grant U2001207, the Project of DEGP (No.2019KCXTD005, 2021ZDZX1068), the Guangdong "Pearl River Talent Recruitment Program"under Grant 2019ZT08X603, RGC under Contract CERG 16203719, 16204820, and Contract R8015, FS112. Kaishun Wu is the corresponding author.

REFERENCES

[1] Alireza Akhbardeh, Bozena Kaminska, and Kouhyar Tavakolian. 2007. BSeg++: A modified blind segmentation method for ballistocardiogram cycle extraction. In *2007 29th Annual International Conference of the IEEE Engineering in Medicine and Biology Society*. IEEE, 1896–1899.

[2] Z. Ali, J. Payton, and V. Sritapan. 2016. At Your Fingertips: Considering Finger Distinctness in Continuous Touch-Based Authentication for Mobile Devices. In *2016 IEEE Security and Privacy Workshops (SPW)*. 272–275.

[3] J Alihanka, K Vaahtoranta, and I Saarikivi. 1981. A new method for long-term monitoring of the ballistocardiogram, heart rate, and respiration. *American Journal of Physiology-Regulatory, Integrative and Comparative Physiology* 240, 5 (1981), R384–R392.

[4] Ahmed A Asaker, Zeinab F Elsharkawy, Sabry Nassar, Nabil Ayad, Osama Zahran, Abd El-Samie, and E Fathi. 2021. A novel cancellable Iris template generation based on salting approach. *Multimedia Tools and Applications* 80, 3 (2021), 3703–3727.

[5] Kim E Barrett, Susan M Barman, Scott Boitano, Heddwen L Brooks, et al. 2016. Ganong's review of medical physiology.

[6] Christoph Bruser, Kurt Stadlthanner, Stijn de Waele, and Steffen Leonhardt. 2011. Adaptive Beat-to-Beat Heart Rate Estimation in Ballistocardiograms. *IEEE Transactions on Information Technology in Biomedicine* 15, 5 (2011), 778–786. https://doi.org/10.1109/TITB.2011.2128337

[7] Carmen Camara, Pedro Peris-Lopez, Lorena Gonzalez-Manzano, and Juan Tapiador. 2018. Real-time electrocardiogram streams for continuous authentication. *Applied Soft Computing* 68 (2018), 784–794.

[8] Yetong Cao, Qian Zhang, Fan Li, Song Yang, and Yu Wang. 2020. PPGPass: nonintrusive and secure mobile two-factor authentication via wearables. In *IEEE INFOCOM 2020-IEEE Conference on Computer Communications*. IEEE, 1917–1926.

[9] Marcus Carlsson, Peter Cain, Catarina Holmqvist, Freddy Stahlberg, Stig Lundback, and Hakan Arheden. 2004. Total heart volume variation throughout the cardiac cycle in humans. *American Journal of Physiology-Heart and Circulatory Physiology* 287, 1 (2004), H243–H250.

[10] GD Clifford, A Shoeb, PE McSharry, and BA Janz. 2005. Model-based filtering, compression and classification of the ECG. *International Journal of Bioelectromagnetism* 7, 1 (2005), 158–161.

[11] Yevgeniy Dodis, Leonid Reyzin, and Adam Smith. 2004. Fuzzy extractors: How to generate strong keys from biometrics and other noisy data. In *International conference on the theory and applications of cryptographic techniques*. Springer, 523–540.

[12] ForgeRock. 2021. 2021 ForgeRock Consumer Identity Breach Report. https://www.forgerock.com/fr/node/226611. Last accessed August 5, 2021.

[13] M. Frank, R. Biedert, E. Ma, I. Martinovic, and D. Song. 2013. Touchalytics: On the Applicability of Touchscreen Input as a Behavioral Biometric for Continuous Authentication. *IEEE Transactions on Information Forensics and Security* 8, 1 (2013), 136–148.

[14] Craig Gentry. 2009. Fully homomorphic encryption using ideal lattices. In *Proceedings of the forty-first annual ACM symposium on Theory of computing*. 169–178.

[15] Hong Guo, Xinrong Cao, Jinghua Wu, and Jintian Tang. 2013. Ballistocardiogram-based person identification using correlation analysis. In *World Congress on Medical Physics and Biomedical Engineering May 26-31, 2012, Beijing, China*. Springer, 570–573.

[16] Nyssa T. Hadgraft, Genevieve N. Healy, Neville Owen, Elisabeth A.H. Winkler, Brigid M. Lynch, Parneet Sethi, Elizabeth G. Eakin, Marj Moodie, Anthony D. LaMontagne, Glen Wiesner, Lisa Willenberg, and David W. Dunstan. 2016. Office workers' objectively assessed total and prolonged sitting time: Individual-level correlates and worksite variations. *Preventive Medicine Reports* 4 (2016), 184–191.

https://doi.org/10.1016/j.pmedr.2016.06.011
[17] John E Hall. 2010. *Guyton and Hall textbook of medical physiology e-Book*. Elsevier Health Sciences.
[18] Joshua Hebert, Brittany Lewis, Hang Cai, Krishna K Venkatasubramanian, Matthew Provost, and Kelly Charlebois. 2018. Ballistocardiogram-based authentication using convolutional neural networks. *arXiv preprint arXiv:1807.03216* (2018).
[19] Norden E Huang, Zheng Shen, Steven R Long, Manli C Wu, Hsing H Shih, Quanan Zheng, Nai-Chyuan Yen, Chi Chao Tung, and Henry H Liu. 1998. The empirical mode decomposition and the Hilbert spectrum for nonlinear and non-stationary time series analysis. *Proceedings of the Royal Society of London. Series A: mathematical, physical and engineering sciences* 454, 1971 (1998), 903–995.
[20] Su Hwan Hwang, Hee Nam Yoon, Yu-Jin G Lee, Do-Un Jeong, Kwang Suk Park, et al. 2013. Nocturnal awakening and sleep efficiency estimation using unobtrusively measured ballistocardiogram. *IEEE transactions on biomedical engineering* 61, 1 (2013), 131–138.
[21] Omer T Inan, Mozziyar Etemadi, Bernard Widrow, Gregory TA Kovacs, et al. 2009. Adaptive cancellation of floor vibrations in standing ballistocardiogram measurements using a seismic sensor as a noise reference. *IEEE transactions on biomedical engineering* 57, 3 (2009), 722–727.
[22] O. T. Inan, P. Migeotte, K. Park, M. Etemadi, K. Tavakolian, R. Casanella, J. Zanetti, J. Tank, I. Funtova, G. K. Prisk, and M. Di Rienzo. 2015. Ballistocardiography and Seismocardiography: A Review of Recent Advances. *IEEE Journal of Biomedical and Health Informatics* 19, 4 (2015), 1414–1427. https://doi.org/10.1109/JBHI.2014.2361732
[23] Abdul Q Javaid, Isaac S Chang, and Alex Mihailidis. 2018. Ballistocardiogram Based Identity Recognition: Towards Zero-Effort Health Monitoring in an Internet-of-Things (IoT) Environment. In *2018 40th Annual International Conference of the IEEE Engineering in Medicine and Biology Society (EMBC)*. IEEE, 3326–3329.
[24] Ari Juels and Madhu Sudan. 2006. A fuzzy vault scheme. *Designs, Codes and Cryptography* 38, 2 (2006), 237–257.
[25] Ari Juels and Martin Wattenberg. 1999. A fuzzy commitment scheme. In *Proceedings of the 6th ACM conference on Computer and communications security*. 28–36.
[26] JustStand.org. 2021. The Fact about Sedentary Lifestyle. https://www.juststand.org/the-facts/. Last accessed August 5, 2021.
[27] Chang-Sei Kim, Andrew M. Carek, Omer T. Inan, Ramakrishna Mukkamala, and Jin-Oh Hahn. 2018. Ballistocardiogram-Based Approach to Cuffless Blood Pressure Monitoring: Proof of Concept and Potential Challenges. *IEEE Transactions on Biomedical Engineering* 65, 11 (2018), 2384–2391. https://doi.org/10.1109/TBME.2018.2797239
[28] Chang-Sei Kim, Andrew M. Carek, Ramakrishna Mukkamala, Omer T. Inan, and Jin-Oh Hahn. 2015. Ballistocardiogram as Proximal Timing Reference for Pulse Transit Time Measurement: Potential for Cuffless Blood Pressure Monitoring. *IEEE Transactions on Biomedical Engineering* 62, 11 (2015), 2657–2664. https://doi.org/10.1109/TBME.2015.2440291
[29] Chang-Sei Kim, Stephanie L Ober, M Sean McMurtry, Barry A Finegan, Omer T Inan, Ramakrishna Mukkamala, and Jin-Oh Hahn. 2016. Ballistocardiogram: Mechanism and potential for unobtrusive cardiovascular health monitoring. *Scientific reports* 6, 1 (2016), 1–6.
[30] Juha M Kortelainen, Martin O Mendez, Anna Maria Bianchi, Matteo Matteucci, and Sergio Cerutti. 2010. Sleep staging based on signals acquired through bed sensor. *IEEE Transactions on Information Technology in Biomedicine* 14, 3 (2010), 776–785.
[31] R.H. Kwong and E.W. Johnston. 1992. A variable step size LMS algorithm. *IEEE Transactions on Signal Processing* 40, 7 (1992), 1633–1642. https://doi.org/10.1109/78.143435
[32] Won Kyu Lee, Heenam Yoon, Chungmin Han, Kwang Min Joo, and Kwang Suk Park. 2016. Physiological signal monitoring bed for infants based on load-cell sensors. *Sensors* 16, 3 (2016), 409.
[33] Hengjian Li, Jian Qiu, and Andrew Beng Jin Teoh. 2020. Palmprint template protection scheme based on randomized cuckoo hashing and MinHash. *Multimedia Tools and Applications* 79, 17 (2020), 11947–11971.
[34] Jingjie Li, Kassem Fawaz, and Younghyun Kim. 2019. Velody: Nonlinear Vibration Challenge-Response for Resilient User Authentication. In *Proceedings of the 2019 ACM SIGSAC Conference on Computer and Communications Security* (London, United Kingdom) *(CCS '19)*. Association for Computing Machinery, New York, NY, USA, 1201–1213. https://doi.org/10.1145/3319535.3354242
[35] Yong Gyu Lim, Ki Hwan Hong, Ko Keun Kim, Jae Hyuk Shin, Seung Min Lee, Gih Sung Chung, Hyun Jae Baek, Do-Un Jeong, and Kwang Suk Park. 2011. Monitoring physiological signals using nonintrusive sensors installed in daily life equipment. *Biomedical engineering letters* 1, 1 (2011), 11–20.
[36] Feng Lin, Chen Song, Yan Zhuang, Wenyao Xu, Changzhi Li, and Kui Ren. 2017. Cardiac Scan: A Non-Contact and Continuous Heart-Based User Authentication System. In *Proceedings of the 23rd Annual International Conference on Mobile Computing and Networking* (Snowbird, Utah, USA) *(MobiCom '17)*. Association for Computing Machinery, New York, NY, USA, 315–328. https://doi.org/10.1145/3117811.3117839
[37] Jian Liu, Cong Shi, Yingying Chen, Hongbo Liu, and Marco Gruteser. 2019. CardioCam: Leveraging Camera on Mobile Devices to Verify Users While Their Heart is Pumping. In *Proceedings of the 17th Annual International Conference on Mobile Systems, Applications, and Services* (Seoul, Republic of Korea) *(MobiSys '19)*. Association for Computing Machinery, New York, NY, USA, 249–261. https://doi.org/10.1145/3307334.3326093
[38] Jonathan Masci, Ueli Meier, Dan Cireşan, and Jürgen Schmidhuber. 2011. Stacked convolutional auto-encoders for hierarchical feature extraction. In *International conference on artificial neural networks*. Springer, 52–59.
[39] P.E. McSharry, G.D. Clifford, L. Tarassenko, and L.A. Smith. 2003. A dynamical model for generating synthetic electrocardiogram signals. *IEEE Transactions on Biomedical Engineering* 50, 3 (2003), 289–294. https://doi.org/10.1109/TBME.2003.808805

[40] Mahesh Kumar Morampudi, Munaga VNK Prasad, Mridula Verma, and USN Raju. 2021. Secure and verifiable iris authentication system using fully homomorphic encryption. *Computers & Electrical Engineering* 89 (2021), 106924.
[41] Mahesh Kumar Morampudi, Munaga VNK Prasad, Mridula Verma, and USN Raju. 2021. Secure and verifiable iris authentication system using fully homomorphic encryption. *Computers & Electrical Engineering* 89 (2021), 106924.
[42] Jorge J Moré. 1978. The Levenberg-Marquardt algorithm: implementation and theory. In *Numerical analysis*. Springer, 105–116.
[43] Ali Moukadem, Azzeddine Finnaoui, Houssem E Gassara, Dominique Adolphe, Laurence Schacher, and Alain Dieterlen. 2018. Time-frequency domain for BCG analysis. In *2018 International Conference on Computer and Applications (ICCA)*. IEEE, 226–230.
[44] I. Odinaka, P. Lai, A. D. Kaplan, J. A. O'Sullivan, E. J. Sirevaag, and J. W. Rohrbaugh. 2012. ECG Biometric Recognition: A Comparative Analysis. *IEEE Transactions on Information Forensics and Security* 7, 6 (2012), 1812–1824.
[45] Sharon Parry and Leon Straker. 2013. The contribution of office work to sedentary behaviour associated risk. *BMC public health* 13, 1 (2013), 1–10.
[46] Eduardo Pinheiro, Octavian Postolache, and Pedro Girão. 2010. Theory and developments in an unobtrusive cardiovascular system representation: ballistocardiography. *The open biomedical engineering journal* 4 (2010), 201.
[47] Paulo Pinto, Bernardo Patrão, and Henrique Santos. 2014. Free Typed Text Using Keystroke Dynamics for Continuous Authentication. In *Communications and Multimedia Security*, Bart De Decker and André Zúquete (Eds.). Springer Berlin Heidelberg, Berlin, Heidelberg, 33–45.
[48] L.R. Rabiner. 1989. A tutorial on hidden Markov models and selected applications in speech recognition. *Proc. IEEE* 77, 2 (1989), 257–286. https://doi.org/10.1109/5.18626
[49] MAURICE B RAPPAPORT, HOWARD B SPRAGUE, and WILLIAM B THOMPSON. 1953. Ballistocardiography: I. physical considerations. *Circulation* 7, 2 (1953), 229–246.
[50] Olaf Ronneberger, Philipp Fischer, and Thomas Brox. 2015. U-net: Convolutional networks for biomedical image segmentation. In *International Conference on Medical image computing and computer-assisted intervention*. Springer, 234–241.
[51] S. J. Shepherd. 1995. Continuous authentication by analysis of keyboard typing characteristics. In *European Convention on Security and Detection, 1995.* 111–114.
[52] JH Shin, BH Choi, YG Lim, DU Jeong, and KS Park. 2008. Automatic ballistocardiogram (BCG) beat detection using a template matching approach. In *2008 30th Annual International Conference of the IEEE Engineering in Medicine and Biology Society*. IEEE, 1144–1146.
[53] Jae Hyuk Shin, Su Hwan Hwang, Min Hye Chang, and Kwang Suk Park. 2011. Heart rate variability analysis using a ballistocardiogram during Valsalva manoeuvre and post exercise. *Physiological measurement* 32, 8 (2011), 1239.
[54] William E Siri. 1956. The gross composition of the body. In *Advances in biological and medical physics*. Vol. 4. Elsevier, 239–280.
[55] Z. Sitová, J. Šeděnka, Q. Yang, G. Peng, G. Zhou, P. Gasti, and K. S. Balagani. 2016. HMOG: New Behavioral Biometric Features for Continuous Authentication of Smartphone Users. *IEEE Transactions on Information Forensics and Security* 11, 5 (2016), 877–892.
[56] C. Song, A. Wang, K. Ren, and W. Xu. 2016. EyeVeri: A secure and usable approach for smartphone user authentication. In *IEEE INFOCOM 2016 - The 35th Annual IEEE International Conference on Computer Communications*. 1–9.
[57] Isaac Starr, AJ Rawson, HA Schroeder, and NR Joseph. 1939. Studies on the estimation of cardiac ouptut in man, and of abnormalities in cardiac function, from the heart's recoil and the blood's impacts; the ballistocardiogram. *American Journal of Physiology-Legacy Content* 127, 1 (1939), 1–28.
[58] Toshiyo Tamura and Y Photoplethysmogram Maeda. 2018. *Seamless healthcare monitoring*. Springer.
[59] Saul A Teukolsky, Brian P Flannery, WH Press, and WT Vetterling. 1992. Numerical recipes in C. *SMR* 693, 1 (1992), 59–70.
[60] María E Torres, Marcelo A Colominas, Gastón Schlotthauer, and Patrick Flandrin. 2011. A complete ensemble empirical mode decomposition with adaptive noise. In *2011 IEEE international conference on acoustics, speech and signal processing (ICASSP)*. IEEE, 4144–4147.
[61] Varonis. 2021. 98 Must-Know Data Breach Statistics for 2021. https://www.varonis.com/blog/data-breach-statistics/. Last accessed August 15, 2021.
[62] F. Wang, Z. Li, and J. Han. 2019. Continuous User Authentication by Contactless Wireless Sensing. *IEEE Internet of Things Journal* 6, 5 (2019), 8323–8331.
[63] Lei Wang, Kang Huang, Ke Sun, Wei Wang, Chen Tian, Lei Xie, and Qing Gu. 2018. Unlock with Your Heart: Heartbeat-Based Authentication on Commercial Mobile Phones. *Proc. ACM Interact. Mob. Wearable Ubiquitous Technol.* 2, 3, Article 140 (Sept. 2018), 22 pages. https://doi.org/10.1145/3264950
[64] Song Wang, Guang Deng, and Jiankun Hu. 2017. A partial Hadamard transform approach to the design of cancelable fingerprint templates containing binary biometric representations. *Pattern Recognition* 61 (2017), 447–458.
[65] Wei Wang, Alex X Liu, and Muhammad Shahzad. 2016. Gait recognition using wifi signals. In *Proceedings of the 2016 ACM International Joint Conference on Pervasive and Ubiquitous Computing*. 363–373.
[66] Lloyd R Welch. 2003. Hidden Markov models and the Baum-Welch algorithm. *IEEE Information Theory Society Newsletter* 53, 4 (2003), 10–13.

[67] Richard M Wiard, Omer T Inan, Brian Argyres, Mozziyar Etemadi, Gregory TA Kovacs, and Laurent Giovangrandi. 2011. Automatic detection of motion artifacts in the ballistocardiogram measured on a modified bathroom scale. *Medical & biological engineering & computing* 49, 2 (2011), 213–220.

[68] Ruqiang Yan and Robert X. Gao. 2008. Rotary Machine Health Diagnosis Based on Empirical Mode Decomposition. *Journal of Vibration and Acoustics* 130, 2 (02 2008). https://doi.org/10.1115/1.2827360 arXiv:https://asmedigitalcollection.asme.org/vibrationacoustics/article-pdf/130/2/021007/5628467/021007_1.pdf 021007.

[69] Xianwen Zhang, Yandong Zhang, Liyan Zhang, Heng Wang, and Jintian Tang. 2018. Ballistocardiogram based person identification and authentication using recurrent neural networks. In *2018 11th International Congress on Image and Signal Processing, BioMedical Engineering and Informatics (CISP-BMEI)*. IEEE, 1–5.

[70] Yongtuo Zhang, Wen Hu, Weitao Xu, Chun Tung Chou, and Jiankun Hu. 2018. Continuous Authentication Using Eye Movement Response of Implicit Visual Stimuli. *Proc. ACM Interact. Mob. Wearable Ubiquitous Technol.* 1, 4, Article 177 (Jan. 2018), 22 pages. https://doi.org/10.1145/3161410

[71] Tianming Zhao, Yan Wang, Jian Liu, Yingying Chen, Jerry Cheng, and Jiadi Yu. 2020. Trueheart: Continuous authentication on wrist-worn wearables using ppg-based biometrics. (2020), 30–39.

[72] Zhidong Zhao, Lei Yang, Diandian Chen, and Yi Luo. 2013. A Human ECG Identification System Based on Ensemble Empirical Mode Decomposition. *Sensors (Basel, Switzerland)* 13, 5 (2013).

A APPENDIX

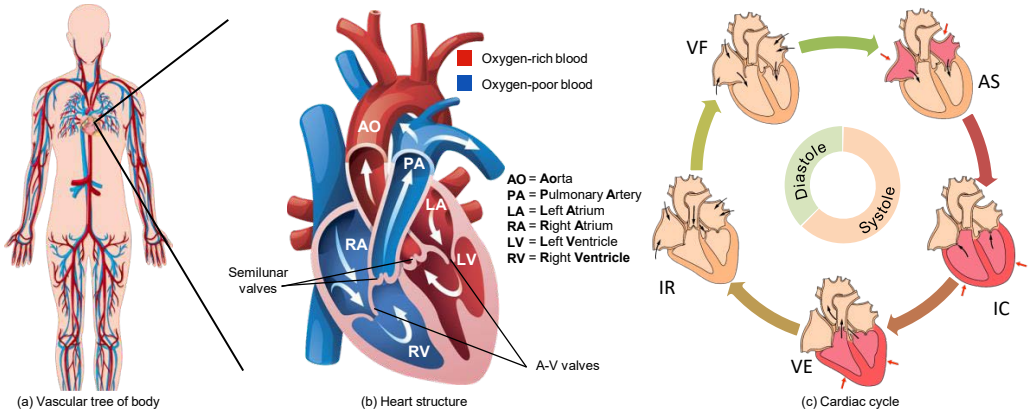

Fig. 20. Illustration of the circulatory system, heart structure and cardiac cycle. The reciprocate motion of heart muscle pumps blood into the circulatory system providing oxygen and nutrients to organs and tissue. To achieve such circulation function, the structure of human heart is designed as two separate pumps as shown in Figure 20: a right heart pumping blood through the lungs (blue part), and a left heart pumping blood through the whole body (red part). Both right and left heart contains a upper chamber (i.e., atria) and a lower chamber (i.e., ventricle). There are atrioventricular (A-V) valves between atrias and ventricles to prevent backflow of blood [5].

The periodic contraction (systole) and relaxation (diastole) of heart can be further illustrated into five major stages[17]: 1) atrial systole (AS), 2) isometric ventricular contraction (IC), 3) ventricular ejection (VE), 4) isometric ventricular relaxation (IR), and 5) ventricular filling (VF). In the stage of atrial systole (AS), atrial contraction causes a rise in intra-atrial pressure and ejects residue blood into the ventricles. Then the isometric ventricular contraction (IC) occurs with an abrupt increase of ventricular pressure caused by the contraction of ventricles. During this stage, the A-V valves and semilunar valves are closed, but the ventricles keep contracting with the ventricular volume unchanged. The ejection (VE) stage begins when the pressure exceed a threshold and push the semilunar valves open. The blood are continuously pumped into lungs and aorta during ventricular systole. At the end of ejection, the ventricular diastole (IR) starts suddenly, decreasing the intra-ventricular pressure in a rapid manner to close the semilunar valves. Then the A-V valves open due to the elevated pressures, and the large amount of blood accumulate in atria fill into the ventricular (VF).

Table 3. Illustration of each wave of a BCG signal

Wave Name	Timing	Description	Wave direction
G	The late stage of AS; Semilunar valves open; Ventricular systole begins	Atrial contraction causes blood flow to rush down to the ventricle, generating a footward force; Not obvious, sometimes disappear	Downward
H	During IC	The ventricular muscles contract and the pressure in the ventricle increases sharply, pushing headward against the A-V valves	Upward
I	The onset of VE	A footward retreat of body provoked by the accelearation of blood into the pulmonary artery and the ascending arch of the aorta	Downward
J	The peak of blood ejection	After the headward movement of the accelerated blood, its impact on the crown of the two aorta arches abruptly reverses the direction of the forces generating the quick recoil of the body in the headward direction	Upward
K	The end of VE Semilunar valves close	K wave is because of systemic circulation that the blood flow is declerated by the peripheral resisitance in the descedning aorta, and the ejection velocity is reduced, resulting in a footward force	Downward
L	The onset of IR A-V valves open	After the closure of semilunar valves, the A-V valve is then lifted up, and the blood in the atrium is given a headward power	Upward
M	Around the onset of VF	The blood flow rushes from the atrium into the ventricle and then hits the apex of the heart, generating footward momentum; A foorward recoil force in the descending aorta	Downward
N	Synchronized with the peak of rapid filling wave (VF)	The deceleration of venous return causing headward body movement	Upward